
Auto Tensor Singular Value Thresholding: A Non-Iterative and Rank-Free Framework for Tensor Denoising

A PREPRINT

© Hiroki Hasegawa

Master's Program in Service Engineering
University of Tsukuba
Tsukuba, Japan
s2420513@u.tsukuba.ac.jp

© Yukihiro Okada

Institute of Systems and Information Engineering,
Center for Artificial Intelligence Research,
Tsukuba Institute for Advanced Research (TIAR)
University of Tsukuba
Tsukuba, Japan
okayu@sk.tsukuba.ac.jp

ABSTRACT

In modern data-driven tasks such as classification, optimization, and forecasting, mitigating the adverse effects of intrinsic noise remains a critical factor in enhancing predictive accuracy. A wide array of denoising and noise reduction techniques has been proposed in response. However, the increasing dimensionality of real-world datasets has exposed the limitations of conventional matrix-based approaches, particularly in preserving the underlying data structure and maintaining analytical precision. These challenges have spurred growing interest in tensor-based methods, which retain multi-way data relationships throughout the analysis process. However, classical tensor decomposition methods often entail substantial computational burden and necessitate both pre-specified ranks and iterative optimization, thereby limiting their practicality. Here, we propose a novel low-rank approximation method for tensor data that eliminates the need for prior rank specification and iterative refinement. Our approach applies statistically grounded singular value thresholding to mode-wise matricizations of a tensor, enabling automatic extraction of significant components while preserving the original multi-dimensional structure. Experimental evaluations demonstrate that our method outperforms existing techniques—such as Higher-Order Singular Value Decomposition (HOSVD), High-Order Orthogonal Iteration (HOOI), and Tucker-L2E—both in terms of estimation accuracy and computational efficiency, particularly in scenarios involving noisy high-dimensional data.

Keywords Multivariate Statistics · Tensor Decomposition · Data Science · Machine Learning

1 Introduction

In recent years, the field of Operations Research has witnessed increasing utilization of real-world data. However, due to limitations in measurement accuracy and external environmental factors, such data inevitably contain noise [1]. A wide range of approaches has been proposed to address the influence of noise in real data, including feature selection techniques to improve classification accuracy, dynamic resampling strategies in evolutionary optimization, wavelet-based enhancements in price forecasting, and models capable of simultaneously estimating short- and long-term inefficiencies [2, 3, 1, 4]. These examples underscore the ubiquity and importance of noise mitigation across various domains, including classification, optimization, forecasting, and efficiency analysis, each of which has prompted the development of domain-specific denoising strategies.

Most existing approaches rely on matrix representations of data. However, as datasets become increasingly high-dimensional—particularly in domains such as sensor networks and biomedical monitoring—the "curse of dimensionality" emerges as a critical challenge. This not only amplifies the computational cost but also compromises structural fidelity during analysis [5]. In particular, transforming high-order tensors into two-dimensional matrices often results in the loss of key internal structures, such as temporal dependencies, spatial correlations, or hierarchical patterns inherent in the original data [6].

In response to these challenges, tensor-based analysis has garnered growing attention due to its ability to preserve multi-way relationships among data modes. Tensors inherently maintain structural characteristics across dimensions, making them well-suited to complex tasks such as demand forecasting and anomaly detection involving temporal, spatial, and attribute interactions [7]. Applications of tensor methods now span a wide range of fields, including sensor integration in smart cities, biomedical signal analysis in healthcare, and compression of high-frequency trading data in financial markets [8]. Tensor-based low-rank approximations are especially valuable for reducing the influence of noise and missing data while achieving accurate predictions [9, 10].

Central to this paradigm is the assumption that signal components are of intrinsically lower rank than noise, enabling noise suppression via low-rank approximations. Various decomposition approaches have been proposed, including CP, Tucker, and Tensor Train (TT) decompositions [11, 12, 13, 14].

CP-based approaches include CP-ALS, Bayesian Robust Tensor Factorization (BRTF), Randomized Block Sampling-CPD, Tensor Robust CP Decomposition, and Randomized CP Decomposition [7, 15, 16, 17, 18]. CP-ALS is a standard approach based on the alternating least squares algorithm, which iteratively updates factor matrices in turn. BRTF is a robust method that estimates low-rank structures while mitigating the influence of outliers through Bayesian inference. Randomized Block Sampling-CPD improves computational efficiency for large-scale tensors by randomly sampling blocks of the tensor. Tensor Robust CP Decomposition is designed to accurately extract low-rank structures even in the presence of sparse outliers. Randomized CP Decomposition employs randomized algorithms to efficiently perform approximate CP decompositions at scale.

Tucker-based methods such as HOSVD, HOOI, HoRPCA variants, TORCA, Zoom-Tucker, and Tucker-L2E are built upon the generalized PCA for higher-order data [19, 20, 21, 22, 17, 23, 24]. Tucker decomposition, a higher-order extension of principal component analysis, offers high flexibility and has inspired numerous variants [7]. HOSVD performs SVD independently on each mode to extract features while preserving tensor structure, whereas HOOI improves approximation accuracy via iterative optimization. HoRPCA-W, HoRPCA-C, and HoRPCA-S introduce various robust losses to suppress outliers, including weighted, Cauchy, and smoothed ℓ_1 losses. TORCA balances orthogonality and robustness, while Zoom-Tucker enables efficient localized decomposition. Tucker-L2E employs ℓ_2 -based optimization for stable, high-rank decomposition even under heavy noise.

TT-based models include TTPUDR, GRIT Decomposition, FastTT, TTOI, and TT-ICE [25, 26, 27, 28, 29]. TT decomposition is a relatively recent alternative to CP and Tucker decompositions, with more limited applications to date. TTPUDR combines TT decomposition with locality-preserving projection for dimensionality reduction while maintaining structural integrity. GRIT Decomposition incorporates graph regularization to capture local structures in a low-rank TT format. FastTT enables fast and accurate decomposition of large-scale, sparse tensors. TTOI alternates forward and backward SVDs to robustly estimate TT structures under noise. TT-ICE incrementally updates TT approximations with theoretical guarantees, balancing compression and efficiency.

While these methods share the goal of low-rank approximation, most require manual rank specification and rely on iterative optimization, which can be computationally expensive and unstable—especially given the NP-hard nature of rank determination [30]. As shown in Table 1, rank estimation and iteration pose practical limitations in many settings.

This study addresses the open question: Can we extract reliable and stable information from noisy high-dimensional data without relying on rank specification or iterative optimization? To this end, we propose Auto Tensor Singular Value Thresholding (ATSV), a novel Tucker-based decomposition method. ATSV applies a statistically grounded singular value thresholding approach, originally proposed for matrices by [31], to each mode unfolding of a tensor. This enables automatic extraction of significant components while maintaining the tensor structure, automatically determines ranks, thereby avoiding manual specification and iterations.

By adaptively selecting thresholds based on mode-wise noise characteristics, ATSV estimates the effective rank statistically, thereby circumventing the NP-hard rank selection problem. Furthermore, by extending the consistency guarantees established in matrix settings to tensors, ATSV provides stable and reproducible estimates that are not affected by initialization choices or convergence-related uncertainties.

To validate our approach, we compare ATSV against (1) HOSVD, the earliest non-iterative Tucker method; (2) HOOI, a standard iterative approach; and (3) Tucker-L2E, a recent nonparametric alternative that also avoids rank specification. Simulation results show that ATSV consistently outperforms these methods in both accuracy and computational efficiency. These advantages are attributed to ATSV’s rank-free, non-iterative design, which simultaneously ensures computational tractability, ease of implementation, and reliable estimation performance.

This paper is organized as follows. Section 2 provides the foundational background, including notation, Tucker decomposition, HOSVD, singular value thresholding, and a detailed description of the proposed method. It also outlines the simulation settings and benchmark methods used for comparison. Section 3 presents quantitative evaluations under

Table 1: Comparison of Tensor Decomposition Methods

Method Name	Fundamentals	1st Author(Year)	Rank Specified?	Iterative?
CP-ALS	CP	Kolda (2009)	Yes	Yes
BRTF	CP	Zhan (2015)	No	Yes
Randomized Block Sampling CPD	CP	Vervliet (2015)	Yes	Yes
Tensor Robust CP Decomposition	CP	Xue (2017)	Yes	Yes
Randomized CP Decomposition	CP	Erichson (2020)	Yes	Yes
HOSVD	Tucker	De Lathauwer (2000a)	Yes	No
HOOI	Tucker	De Lathauwer (2000b)	Yes	Yes
HoRPCA-W	Tucker	Tomioka (2011)	No	Yes
HoRPCA-C	Tucker	Goldfarb (2014)	Yes	Yes
HoRPCA-S	Tucker	Goldfarb (2014)	No	Yes
TORCA	Tucker	Xue (2017)	Yes	Yes
Zoom-Tucker	Tucker	Jang (2021)	Yes	Yes
Tucker-L2E	Tucker	Heng (2023)	No	Yes
ATSV	Tucker	Hasegawa (2025)	No	No
TTPUDR	TT	Bai (2019)	Yes	Yes
GRTT Decomposition	TT	Sofuoglu (2020)	Yes	Yes
FastTT	TT	Li (2020)	Yes	Yes
TTOI	TT	Zhou (2022)	Yes	Yes
TT-ICE	TT	Aksoy (2024)	No	Yes

three signal-to-noise ratio (SNR) conditions: high, moderate, and low. Section 4 discusses the implications of the results, offering both theoretical insights and practical implications. Section 5 concludes the study and outlines directions for future work. Supplementary materials provide technical derivations.

2 Methodology

This section introduces the foundational components of our proposed method: (1) notation, (2) Tucker decomposition, (3) Higher-Order Singular Value Decomposition (HOSVD), (4) Singular Value Thresholding (SVT), and (5) the proposed method.

2.1 Notation

Throughout this paper, tensors are denoted by calligraphic uppercase letters such as \mathcal{X}, \mathcal{G} and are assumed to be of order three or higher. Matrices are denoted by bold uppercase letters, e.g., \mathbf{U}, \mathbf{V} , vectors by bold lowercase letters, e.g., \mathbf{u}, \mathbf{v} , and scalars by Roman or Greek characters such as x, y, z, λ, σ . For an N -way tensor $\mathcal{X} \in \mathbb{R}^{I_1 \times \dots \times I_N}$, its mode- n unfolding is denoted as $\mathbf{X}_{(n)} \in \mathbb{R}^{I_n \times (I_1 \dots I_{n-1} I_{n+1} \dots I_N)}$, where the mode- n indices form the rows and all other mode indices are flattened into columns.

2.2 Tucker Decomposition

Tucker decomposition factorizes a given tensor $\mathcal{X} \in \mathbb{R}^{I_1 \times \dots \times I_N}$ into a core tensor and a set of factor matrices:

$$\mathcal{X} \approx \mathcal{G} \times_1 \mathbf{U}^{(1)} \times_2 \dots \times_N \mathbf{U}^{(N)},$$

where $\mathcal{G} \in \mathbb{R}^{R_1 \times \dots \times R_N}$ is the core tensor containing compressed information, and $\mathbf{U}^{(n)} \in \mathbb{R}^{I_n \times R_n}$ are the factor matrices corresponding to each mode. The n -mode product of a tensor $\mathcal{A} \in \mathbb{R}^{I_1 \times \dots \times I_N}$ and a matrix $\mathbf{U}^{(n)} \in \mathbb{R}^{J \times I_n}$ is defined as:

$$\mathcal{B}_{i_1, \dots, i_{n-1}, j, i_{n+1}, \dots, i_N} = \sum_{i_n=1}^{I_n} \mathcal{A}_{i_1, \dots, i_n, i_{n+1}, \dots, i_N} \cdot \mathbf{U}_{j, i_n}^{(n)}.$$

2.3 HOSVD

The Higher-Order Singular Value Decomposition (HOSVD) is a type of Tucker decomposition that employs orthogonal matrices as factor matrices. It decomposes a tensor $\mathcal{X} \in \mathbb{R}^{I_1 \times \dots \times I_N}$ as:

$$\mathcal{X} = \mathcal{G} \times_1 \mathbf{U}^{(1)} \times_2 \dots \times_N \mathbf{U}^{(N)},$$

where $\mathbf{U}^{(n)}$ are obtained by applying SVD to the mode- n unfolding $\mathbf{X}_{(n)}$ of the tensor, and \mathcal{G} is computed by:

$$\mathcal{G} = \mathcal{X} \times_1 \left(\mathbf{U}^{(1)} \right)^\top \times_2 \dots \times_N \left(\mathbf{U}^{(N)} \right)^\top.$$

HOSVD guarantees orthogonality in each mode. However, because it applies SVD independently to each mode, it does not necessarily yield the optimal compression across mode interactions [19].

2.4 Singular Value Thresholding

Consider the observation model:

$$\mathbf{Y}_n = \mathbf{X}_n + \sigma \mathbf{Z}_n, \quad (1)$$

where $\mathbf{X}_n \in \mathbb{R}^{m \times n}$ is a true low-rank matrix, $\sigma > 0$ is the noise level, and \mathbf{Z}_n is a noise matrix with entries drawn independently from the standard normal distribution $\mathcal{N}(0, 1)$. The singular value decomposition (SVD) of the observation matrix \mathbf{Y}_n is:

$$\mathbf{Y}_n = \sum_{i=1}^m y_{n,i} \mathbf{u}_{n,i} \mathbf{v}_{n,i}^\top,$$

where $y_{n,1} \geq y_{n,2} \geq \dots \geq y_{n,m}$ are the singular values, and $\mathbf{u}_{n,i}, \mathbf{v}_{n,i}$ are the left and right singular vectors, respectively. The true matrix \mathbf{X}_n has a fixed decomposition:

$$\mathbf{X}_n = \sum_{i=1}^{r_{\max}} x_i \mathbf{a}_i \mathbf{b}_i^\top, \quad (2)$$

with $x_1 \geq x_2 \geq \dots \geq x_{r_{\max}} > 0$ being the singular values and $\mathbf{a}_i, \mathbf{b}_i$ being fixed singular vectors.

To estimate \mathbf{X}_n from the noisy observation \mathbf{Y}_n , we apply singular value thresholding (SVT) with a threshold τ , resulting in:

$$\hat{\mathbf{X}}_{n,\tau} = \sum_{i=1}^m \eta_H(y_{n,i}; \tau) \mathbf{u}_{n,i} \mathbf{v}_{n,i}^\top, \quad \eta_H(y_{n,i}; \tau) = y_{n,i} \cdot \mathbf{1}_{\{y_{n,i} \geq \tau\}}, \quad (3)$$

where $\mathbf{1}_{\{y_{n,i} \geq \tau\}}$ is the indicator function.

If the noise level σ and the matrix size n are known and $m = n$, Gavish and Donoho (2014) provide the optimal threshold:

$$\tau^* = \frac{4}{\sqrt{3}} \cdot \sqrt{n} \sigma.$$

For rectangular matrices, the optimal threshold uses the aspect ratio $\beta = m/n$:

$$\tau^* = \lambda^*(\beta) \cdot \sqrt{n} \sigma, \quad \lambda^*(\beta) = \frac{\sqrt{2(\beta+1) + 8\beta}}{(\beta+1) + \sqrt{\beta^2 + 14\beta + 1}}.$$

When σ is unknown, it can be estimated from the data using:

$$\hat{\sigma}(\mathbf{Y}_n) = \frac{y_{\text{med}}}{\sqrt{n \cdot \mu_\beta}}.$$

where y_{med} is the median singular value of \mathbf{Y}_n and μ_β is the median of the Marčenko–Pastur distribution. This estimator satisfies the asymptotic property:

$$\lim_{n \rightarrow \infty} \frac{\hat{\sigma}(\mathbf{Y}_n)}{1/\sqrt{n}} = 1 \quad (\text{a.s.}) \quad (4)$$

For theoretical underpinnings of SVT and its statistical justification, we refer the reader to Appendix 8.1 and the AMSE derivation in Appendix 8.2.

2.5 Proposed Method: Auto Tensor Singular Value Thresholding (ATSV)

We consider the following observation model for tensors:

$$\mathcal{Y} = \mathcal{X} + \sigma\mathcal{E}, \quad \text{Rank}(\mathcal{X}) = (R_{I_1}, \dots, R_{I_N}), \quad 0 < R_{I_k} \leq I_k, \quad (5)$$

where $\mathcal{Y} \in \mathbb{R}^{I_1 \times \dots \times I_N}$ is the observed noisy tensor, \mathcal{X} is the underlying low-rank tensor, σ is the noise level, and \mathcal{E} is a random noise tensor with i.i.d. standard Gaussian entries. Tucker rank is used to describe the multilinear rank of \mathcal{X} , defined via the mode- k unfoldings as:

$$R_{I_k} = \text{Rank}(\mathbf{X}_{(k)}).$$

Our goal is to estimate \mathcal{X} from \mathcal{Y} . To do so, we perform SVD on each mode- k unfolding $\mathbf{Y}_{(k)}$ of the observed tensor and apply singular value thresholding to identify significant components. The Tucker core of the observed tensor is given by:

$$\mathcal{S}_y = \mathcal{Y} \times_1 (\mathbf{U}^{(1)})^\top \times_2 \dots \times_N (\mathbf{U}^{(N)})^\top,$$

with orthonormal matrices $\mathbf{U}^{(k)}$ obtained from the left singular vectors of $\mathbf{Y}_{(k)}$. The true core \mathcal{S}_x and corresponding bases $\mathbf{A}^{(k)}$ are similarly defined.

From the unfolding matrices:

$$\mathbf{Y}_{(k)} = \sum_{i=1}^{d_{(k)}^*} y_{(k),i} \mathbf{u}_{(k),i} \mathbf{v}_{(k),i}^\top, \quad \mathbf{X}_{(k)} = \sum_{i=1}^{R_{I_k}} x_{(k),i} \mathbf{a}_{(k),i} \mathbf{b}_{(k),i}^\top,$$

with $d_{(k)}^* = \prod_{l \neq k} I_l$, we define the noise model for matrices:

$$\mathbf{Y}_{(k)} = \mathbf{X}_{(k)} + \sigma \mathbf{E}_{(k)}, \quad (6)$$

where $\mathbf{E}_{(k)}$ is the mode- k unfolding of the noise tensor \mathcal{E} .

Using the SVT approach described earlier, the estimate of the denoised unfolding $\hat{\mathbf{X}}_{(k)}$ is given by:

$$\hat{\mathbf{X}}_{(k), \tau_{(k)}^*} = \sum_{i=1}^{d_{(k)}^*} \eta_H(y_{(k),i}; \tau_{(k)}^*) \mathbf{u}_{(k),i} \mathbf{v}_{(k),i}^\top, \quad \tau_{(k)}^* = \omega(\beta_{(k)}) \cdot y_{(k),\text{med}}, \quad (7)$$

where $\beta_{(k)} = I_k/d_{(k)}^*$ is the aspect ratio and $y_{(k),\text{med}}$ is the median singular value.

Subsequently, the denoised tensor is reconstructed using only the top $g_{(k)}$ components:

$$\hat{\mathbf{U}}^{(k)} = [\mathbf{u}_{(k),1}, \dots, \mathbf{u}_{(k),g_{(k)}}], \quad \hat{\mathbf{V}}^{(k)} = [\mathbf{v}_{(k),1}, \dots, \mathbf{v}_{(k),g_{(k)}}].$$

Finally, the low-rank tensor estimate $\hat{\mathcal{X}}$ is reconstructed as:

$$\hat{\mathcal{X}} = \hat{\mathcal{S}}_y \times_1 \hat{\mathbf{U}}^{(1)} \times_2 \dots \times_N \hat{\mathbf{U}}^{(N)}, \quad \hat{\mathcal{S}}_y = \mathcal{Y} \times_1 (\hat{\mathbf{U}}^{(1)})^\top \times_2 \dots \times_N (\hat{\mathbf{U}}^{(N)})^\top.$$

The proposed method, Auto Tensor Singular Value Thresholding (ATSV), avoids the pitfalls of traditional HOSVD by statistically determining the rank for each mode through thresholding, does not rely on prior rank specification or iterative optimization. Its theoretical foundation is supported by statistical results in Appendix 8.1 and 8.2. Moreover, an overview of the proposed method is presented in Fig. 1. As illustrated in this figure, the computation proceeds through three major steps. First, the observed tensor is unfolded into multiple matrices. Second, for each unfolded matrix, a threshold is calculated to separate the true signal from noise, and the significant signal components are extracted. Finally, the tensor is reconstructed from the denoised matrices to obtain an estimate of the true data.

Algorithm 1 summarizes the procedure, and details regarding the threshold calibration, noise estimation, and integral computation are provided in Appendices 8.3.1, 8.3.2, and 8.3.3, respectively.

3 Simulation

This section describes the simulation framework used to evaluate the performance of the proposed method, ATSV, along with the baseline methods. We first introduce the overall design of the simulation, then outline the algorithms of HOOI and Tucker-L2E. HOSVD has already been discussed in Section 2.3 and is omitted here.

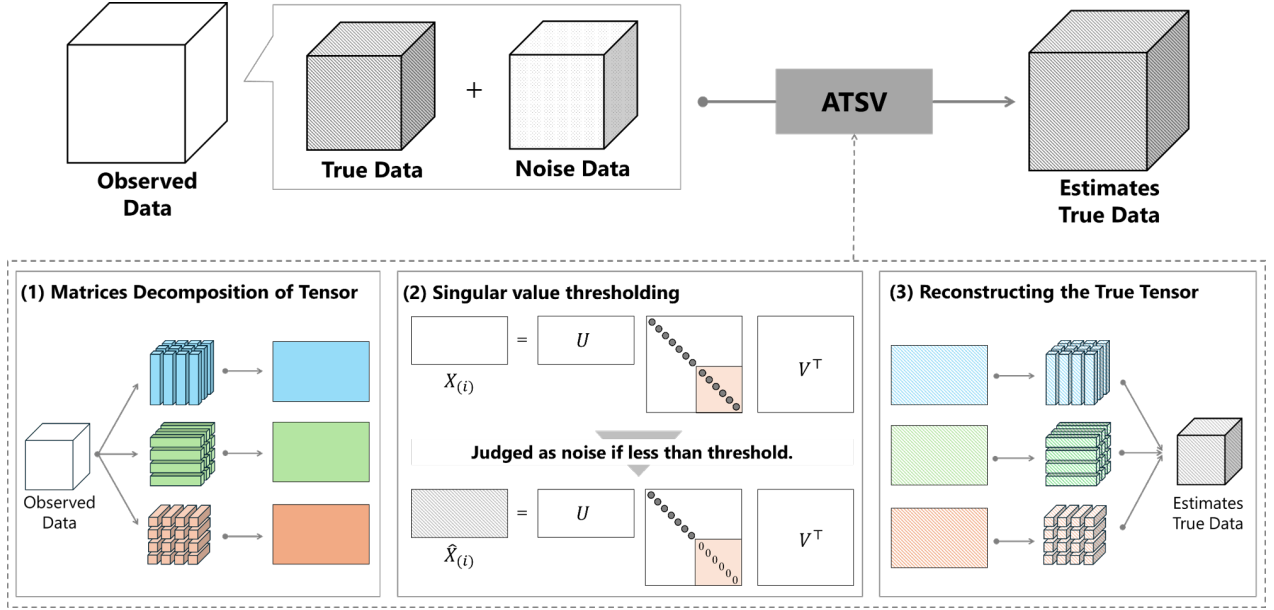


Figure 1: Overview of the proposed method

Algorithm 1 Auto Tensor Singular Value Thresholding (ATSV)**Input:** Observed tensor \mathcal{X} , noise flag `sigma_known`, noise level σ (if known)**Output:** Denoised tensor $\hat{\mathcal{X}}$

-
- 1: $d \leftarrow$ number of modes of \mathcal{X}
 - 2: Initialize rank list $\mathbf{r} \leftarrow []$
 - 3: **for** $k = 1$ to d **do**
 - 4: $\mathbf{X}_{(k)} \leftarrow$ mode- k unfolding of \mathcal{X}
 - 5: $(m, n) \leftarrow$ shape of $\mathbf{X}_{(k)}$, $\beta \leftarrow m/n$
 - 6: Compute SVD: $\mathbf{X}_{(k)} = \mathbf{U}\mathbf{S}\mathbf{V}^\top$
 - 7: **if** `sigma_known` is True **then**
 - 8: $\tau \leftarrow \text{OPTIMALSVHTCOEF}(\beta, \text{True}) \cdot \sqrt{n} \cdot \sigma$
 - 9: **else**
 - 10: $\tau \leftarrow \text{OPTIMALSVHTCOEF}(\beta, \text{False}) \cdot \text{median}(\mathbf{S})$
 - 11: **end if**
 - 12: $r_k \leftarrow \max(1, \#\{i \mid S_i > \tau\})$
 - 13: Append r_k to \mathbf{r}
 - 14: **end for**
 - 15: Compute truncated Tucker decomposition of \mathcal{X} with ranks \mathbf{r} :
 - 16: $(\mathcal{G}, \{\mathbf{U}^{(k)}\}_{k=1}^d) \leftarrow \text{TUCKER}(\mathcal{X}, \mathbf{r})$
 - 17: $\hat{\mathcal{X}} \leftarrow \mathcal{G} \times_1 \mathbf{U}^{(1)} \times_2 \cdots \times_d \mathbf{U}^{(d)}$
 - 18: **return** $\hat{\mathcal{X}}$
-

3.1 Simulation Setup

We evaluate the accuracy and efficiency of each method by varying the Tucker rank and SNR. The SNR is defined as [33]:

$$\text{SNR} = \frac{\lambda_{\min}}{\sigma}, \quad (8)$$

where λ_{\min} is the smallest non-zero singular value and σ denotes the noise level. Following [33], we categorize SNR into three regimes: strong ($\alpha \geq 3/4$), moderate ($1/2 \leq \alpha < 3/4$), and weak ($\alpha < 1/2$), where $\lambda_{\min}/\sigma = p^\alpha$. HOOI is known to be optimal in the strong SNR regime, while maximum likelihood estimation is theoretically optimal for moderate SNRs, though impractical due to computational constraints. No consistent estimator is known for the weak SNR regime, where signals are deeply buried in noise.

To generate synthetic tensors, we first construct a random tensor \mathcal{W} and retain only the top components corresponding to the target Tucker rank (R, R, R) to form the true low-rank tensor \mathcal{X} . The observed tensor \mathcal{Y} is then created by adding scaled Gaussian noise:

$$\mathcal{Y} = \mathcal{X} + \sigma\mathcal{E}, \quad \mathcal{X}, \mathcal{Y}, \mathcal{E} \in \mathbb{R}^{50 \times 50 \times 50}.$$

Tucker rank values range from $(5, 5, 5)$ to $(45, 45, 45)$, and 100 trials are conducted for each condition. The noise scale σ is randomly sampled from the standard normal distribution. The relative error (RE) and mean computation time are used for evaluation. The RE is defined as:

$$\text{RE} = \frac{\|\mathcal{X} - \hat{\mathcal{X}}\|_F}{\|\mathcal{X}\|_F},$$

where $\|\cdot\|_F$ is the Frobenius norm. Lower RE values indicate superior estimation performance.

Simulations were conducted on a Windows 11 Pro 64-bit PC with an Intel Core i9-12900KF processor and 64 GB RAM. Python 3.9.18 was used with NumPy 1.26.4 and TensorLy 0.8.1. Baselines include HOSVD, HOOI, three Tucker-L2E variants (with Spectral, ALS, and HOSVD initializations), and the proposed ATSV. For HOOI, the maximum number of iterations was set to 1000 and convergence tolerance to 10^{-6} . The Tucker-L2E implementation is a Python translation of the original C-based code from [24].

3.2 Overview of HOOI

The Higher-Order Orthogonal Iteration (HOOI) algorithm aims to compute a low-rank Tucker approximation of a given tensor $\mathcal{X} \in \mathbb{R}^{I_1 \times \dots \times I_N}$ with a specified multilinear rank (R_1, \dots, R_N) . It iteratively updates factor matrices $\mathbf{U}^{(n)} \in \mathbb{R}^{I_n \times R_n}$ to minimize the reconstruction error.

The algorithm begins with initial factor matrices obtained by applying truncated SVD to each mode- n unfolding $\mathbf{X}_{(n)}$ and extracting the top R_n left singular vectors. At each iteration, it updates one factor matrix $\mathbf{U}^{(n)}$ at a time by fixing all other modes and projecting the tensor as:

$$\mathcal{M}^{(n)} = \mathcal{X} \times_{k \neq n} \left(\mathbf{U}^{(k)} \right)^\top,$$

where $\times_{k \neq n}$ denotes successive mode- k products over all modes except n . Then, the mode- n unfolding $\mathbf{M}_{(n)}$ is decomposed via SVD, and the top R_n left singular vectors are used to update $\mathbf{U}^{(n)}$. This process is repeated for all modes until convergence, which is typically assessed via change in factor matrices or approximation error.

Once the factor matrices are determined, the core tensor is computed as:

$$\mathcal{G} = \mathcal{X} \times_1 \left(\mathbf{U}^{(1)} \right)^\top \times_2 \dots \times_N \left(\mathbf{U}^{(N)} \right)^\top.$$

The resulting approximation is given by:

$$\hat{\mathcal{X}} = \mathcal{G} \times_1 \mathbf{U}^{(1)} \times_2 \dots \times_N \mathbf{U}^{(N)}.$$

HOOI can be viewed as a tensor generalization of the orthogonal iteration method, leveraging successive projection and subspace optimization. Since it requires manual rank specification, we follow the strategy from [?], selecting the smallest R_n such that the cumulative energy (sum of singular values) exceeds 90% of the total in mode- n .

3.3 Overview of Tucker-L2E

Tucker-L2E is a robust tensor decomposition method designed to estimate a low-rank tensor \mathcal{L} from an observed tensor \mathcal{X} that may include sparse outliers \mathcal{S} and dense noise \mathcal{E} [24]. The generative model is:

$$\mathcal{X} = \mathcal{L} + \mathcal{S} + \mathcal{E},$$

where \mathcal{L} has a low Tucker rank, \mathcal{S} is sparse, and \mathcal{E} is dense noise. Tucker-L2E minimizes the following L2E-based loss function:

$$h_{\Omega}(\mathcal{L}, \tau) = \frac{|\Omega|}{2\pi\tau} - \frac{1}{\pi\tau} \sum_{(i_1, \dots, i_N) \in \Omega} \exp\left(-\frac{\tau^2}{2} (\mathcal{X}_{i_1, \dots, i_N} - \mathcal{L}_{i_1, \dots, i_N})^2\right),$$

where Ω is the set of observed entries, and $\tau > 0$ is a precision parameter. The exponential term corresponds to the likelihood under Gaussian noise, yielding robustness against outliers. The optimization is solved via L-BFGS-B, enforcing positivity of τ through $\tau = \exp(\eta)$.

We evaluate three initialization schemes provided in [24]: (1) HOSVD initialization, which imputes missing values with the mean and performs HOSVD; (2) ALS-based HOOI initialization, which iteratively refines HOSVD outputs via alternating optimization; (3) Spectral initialization with diagonal deletion, which performs SVD after removing diagonal elements to mitigate bias from self-correlations. These schemes are chosen to enhance Tucker-L2E’s robustness across different data structures and noise levels.

4 Results

4.1 Figure Composition

Figures 2 through 4 illustrate, under each SNR condition, (A) the mean of the relative error, (B) the standard deviation of the relative error, (C) the mean of the empirical computation time, and (D) the standard deviation of the empirical computation time. The horizontal axis in each panel denotes the true rank, while the red dashed lines in panels (B) and (D) indicate a reference value corresponding to a standard deviation of 1. The legend is consolidated in panel (A). All vertical axes are presented on a logarithmic scale.

4.2 Results under Strong SNR

Figure 2(A) shows that HOSVD consistently yields relative errors above 25, often exceeding 30 except at rank 5, indicating poor estimation accuracy under moderate noise conditions. Tucker-L2E variants exhibit a monotonic decline in error with increasing rank. ATSV maintains low and stable error levels across all ranks and achieves superior accuracy for ranks between 5 and 30. Around rank 30, ATSV, HOOI, and Tucker-L2E (ALS) converge in performance, after which Tucker-L2E exhibits the lowest error.

Regarding estimation variability, Figure 2(B) indicates that HOSVD exceeds a standard deviation of 1 at all ranks, highlighting poor reproducibility. In contrast, Tucker-L2E variants, HOOI, and ATSV remain consistently below this threshold, suggesting greater stability. Notably, ATSV achieves the lowest standard deviations across most ranks, demonstrating highly consistent performance.

As for computation time, Figure 2(C) identifies HOOI as the most computationally expensive method, requiring up to 40 seconds per run. HOSVD is the fastest, averaging approximately 0.1 seconds. ATSV ranks second in speed, averaging around 0.2 seconds and outperforming all Tucker-L2E implementations. Figure 2(D) further confirms that HOOI exhibits high computation time variability, while the other methods—including ATSV—maintain standard deviations around 10^{-2} , indicating stable computational performance.

4.3 Results under Moderate SNR

Figure 3(A) shows that HOSVD produces relative errors consistently exceeding 30%, underperforming all other methods. ATSV demonstrates a steady decrease in error as rank increases, and intersects the performance curves of HOOI and Tucker-L2E near rank 35. It achieves the highest accuracy for ranks between 5 and 35, while Tucker-L2E becomes the most accurate beyond rank 35.

Figure 3(B) indicates that HOSVD exhibits standard deviations above 1 across all ranks, reflecting unstable estimates. In contrast, Tucker-L2E, HOOI, and ATSV show values below 1, suggesting stable performance. Among them, ATSV provides the lowest variability across a wide range of ranks, although the variances are slightly larger than those observed in Figure 2(B), likely due to the weaker SNR setting.

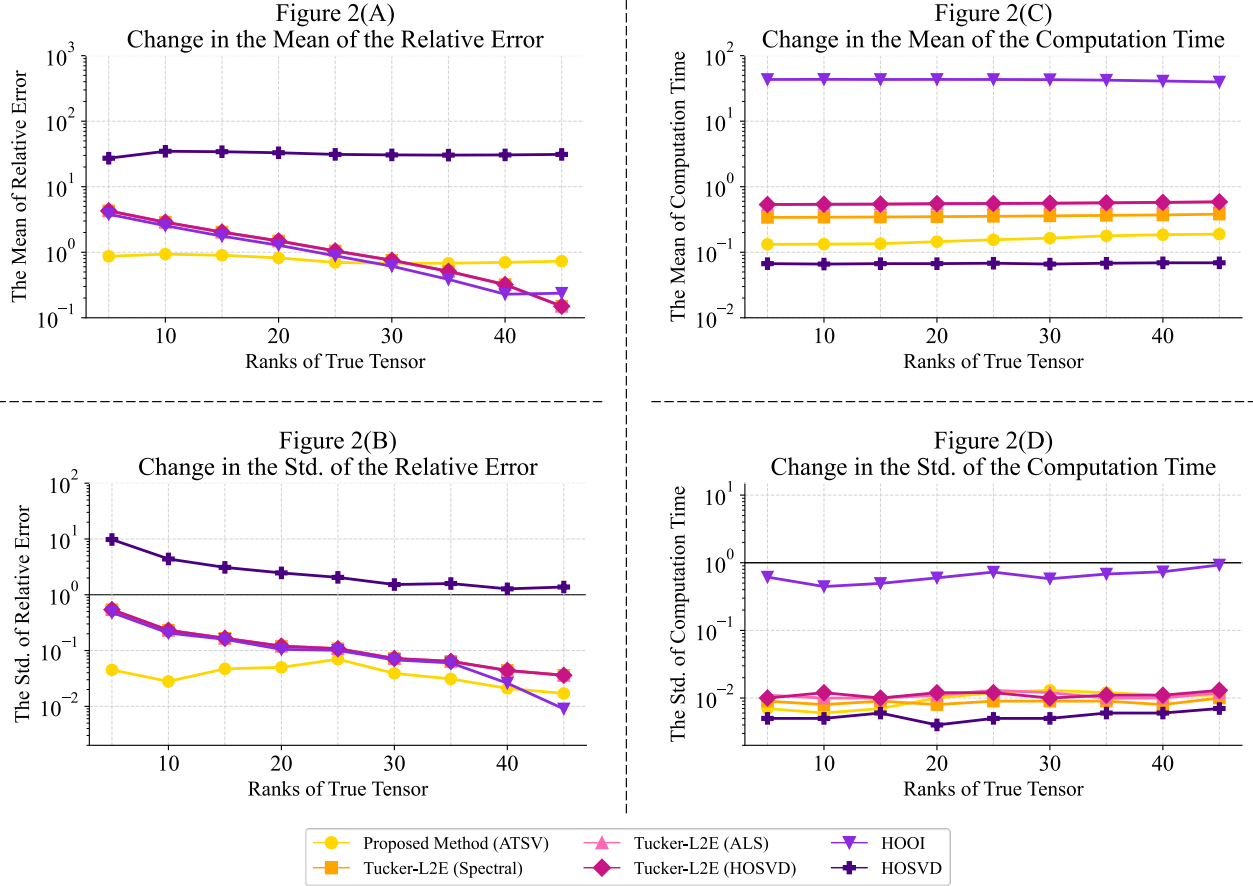


Figure 2: Results under strong SNR

This figure shows the mean and standard deviation of relative error and computation time under strong SNR across 100 trials. Each method is evaluated with increasing true rank from 5 to 45.

In Figure 3(C), HOOI has the highest computational cost (up to 42 seconds), whereas ATSV remains the second fastest method after HOSVD, with a mean computation time around 0.2 seconds. Figure 3(D) supports these findings by showing that HOOI’s computation time fluctuates considerably at some ranks, while ATSV maintains consistent performance, similar to the strong SNR case.

4.4 Results under Weak SNR

Figure 4(A) illustrates the substantial impact of strong noise on HOSVD, with relative errors peaking near 160 around rank 10. In contrast, ATSV maintains the lowest error across most ranks, demonstrating robust noise resistance. Although the performance gap narrows at rank 45, ATSV continues to outperform other methods at lower ranks.

Figure 4(B) shows that HOSVD yields high standard deviations across all ranks, indicating unstable estimates. While Tucker-L2E and HOOI also exhibit variances exceeding 1 at certain ranks—unlike in previous SNR settings—ATSV remains below 1 throughout, except for a modest increase after rank 35. These results underscore ATSV’s consistent estimation stability under severe noise conditions.

In Figure 4(C), HOOI exhibits the longest computation time, reaching up to 47 seconds per trial. Although Tucker-L2E shows slightly increased computation times compared to previous SNR conditions, ATSV and HOSVD retain stable computation times, with ATSV averaging around 0.2 seconds. Figure 4(D) further supports these findings: HOOI shows large computation time variability, and Tucker-L2E displays elevated fluctuations at low ranks (e.g., rank 5). In contrast, ATSV exhibits low standard deviation across all ranks, indicating stable and predictable computational performance.

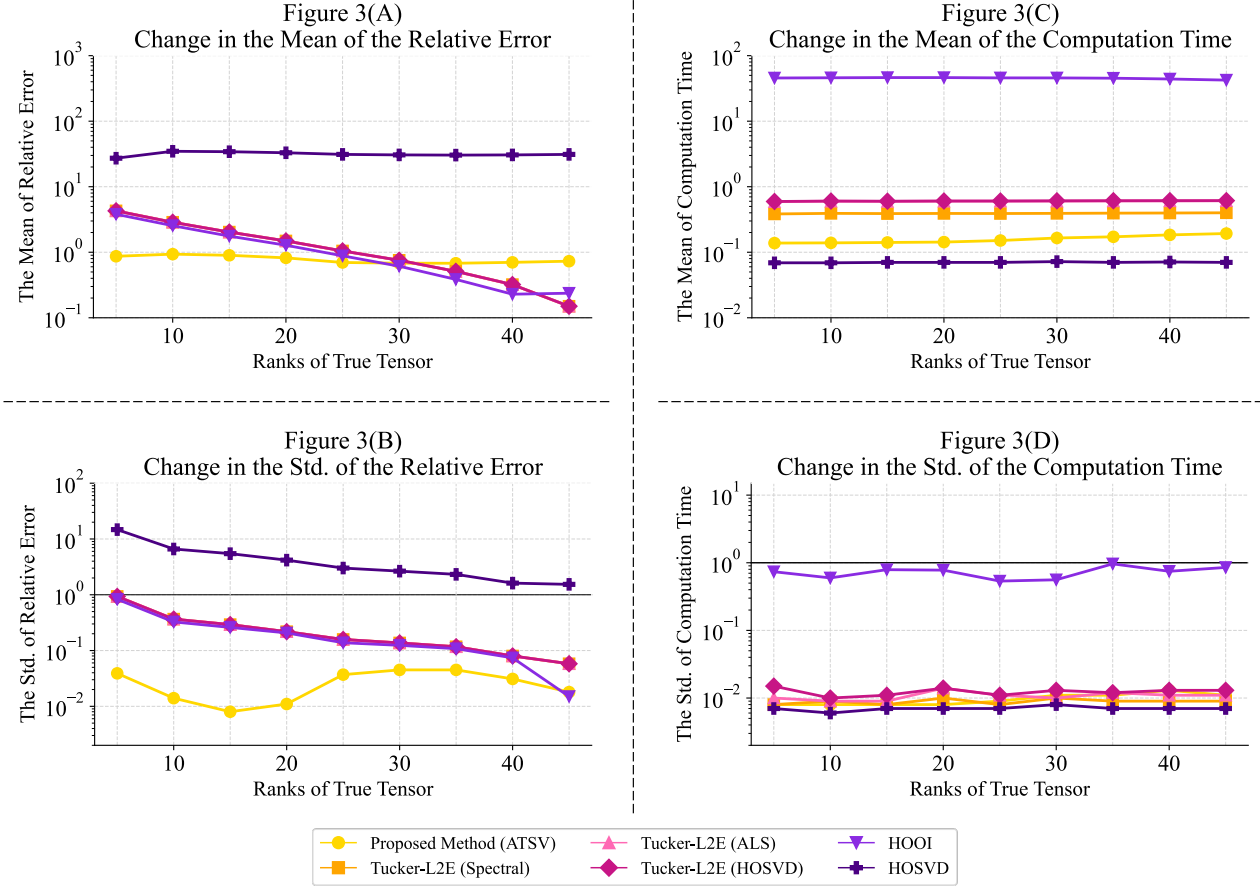


Figure 3: Results under moderate SNR

This figure shows the mean and standard deviation of relative error and computation time under moderate SNR across 100 trials. Each method is evaluated with increasing true rank from 5 to 45.

5 Discussion

In this study, we proposed a non-iterative and rank-free tensor decomposition method, Auto Tensor Singular Value Thresholding (ATSV), and conducted comparative evaluations with existing methods under three different SNR conditions. The results demonstrated that ATSV achieves a high level of performance in terms of estimation accuracy, stability, and computational efficiency, and maintains an excellent overall balance across these aspects.

With regard to estimation accuracy, ATSV consistently achieved low relative errors under all tested conditions. It outperformed HOSVD across the board and showed comparable or superior accuracy to Tucker-L2E and HOOI, particularly under low- to moderate-rank settings. This stability in performance, even under lower SNR conditions, can be attributed to ATSV’s use of statistically derived singular value thresholds, which enable effective separation of signal from noise without extracting irrelevant components. By adapting to the signal-to-noise characteristics in each mode-unfolded matrix, ATSV effectively distinguishes meaningful signals from noise, thereby preventing the inclusion of irrelevant components that degrade estimation accuracy—an issue commonly encountered in other decomposition methods under high-noise conditions or when the rank is incorrectly specified. To ensure fair comparison, all methods were evaluated under consistent initialization settings, parameter tuning procedures, and input dimensions. This provides confidence that the observed advantages of ATSV are intrinsic to the method rather than artifacts of experimental design.

In terms of stability, ATSV does not require iterative optimization or prior rank specification. By applying thresholding directly to the mode-unfolded matrices using a statistically grounded approach, it avoids sensitivity to initial values and convergence criteria, which helps achieve consistent and reproducible results. Although a slight increase in standard deviation was observed under extremely low SNR conditions with increasing rank, the relative error remained low

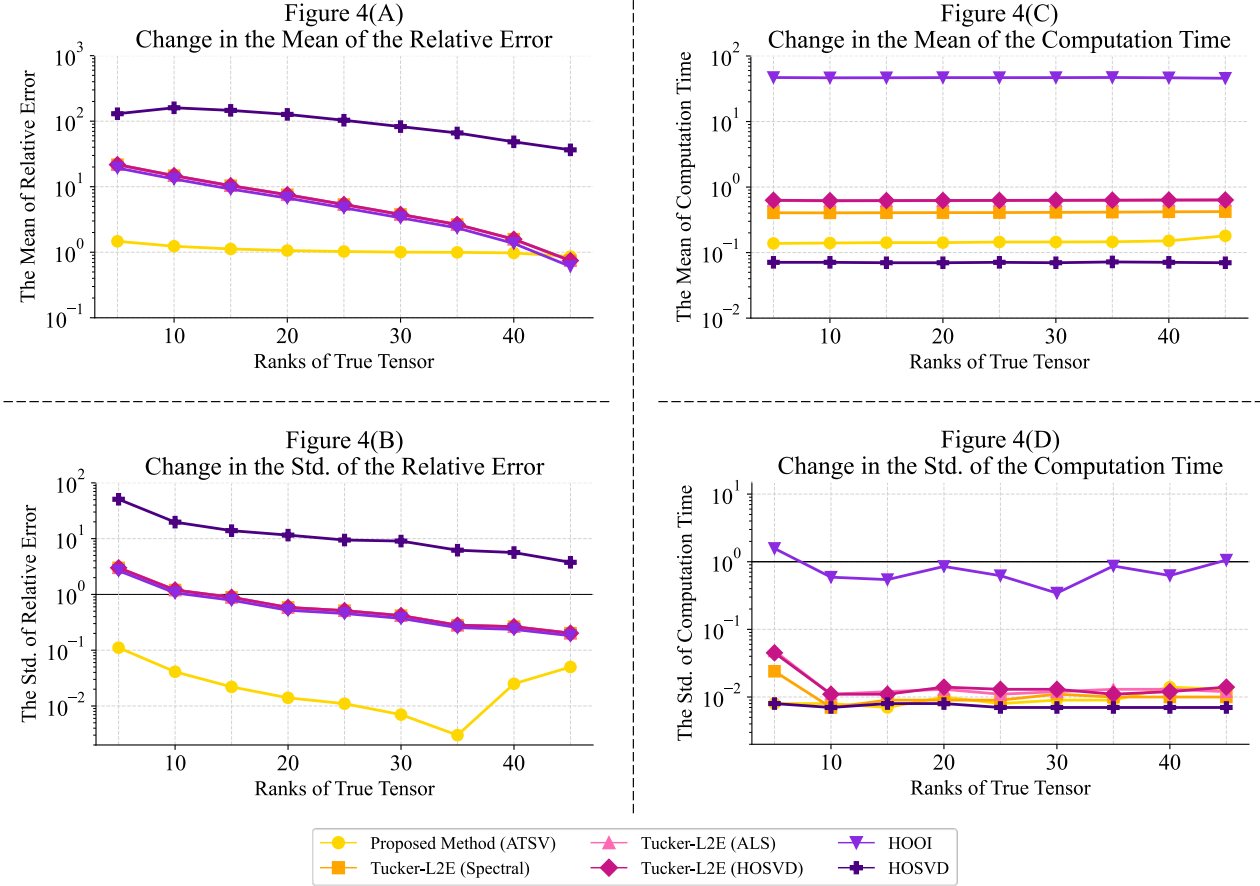


Figure 4: Results under weak SNR

This figure shows the mean and standard deviation of relative error and computation time under weak SNR across 100 trials. Each method is evaluated with increasing true rank from 5 to 45.

and the overall variance was still smaller than that of competing methods. This finding indicates that the proposed method maintains stable performance even in scenarios where traditional methods exhibit reduced reliability due to noise contamination or optimization-related challenges.

From the viewpoint of computational efficiency, ATSV offers a clear advantage. Unlike iterative methods such as HOOI and Tucker-L2E, its non-iterative nature enables substantially faster processing. The empirical results showed that while HOOI and Tucker-L2E required longer computation times as noise levels increased, ATSV consistently completed in under 0.2 seconds, regardless of the noise conditions. This aspect is particularly important for large-scale or time-sensitive applications, where long computation times may limit practical utility. This efficiency stems from its non-iterative design, which eliminates the need for repeated updates or convergence checks, thereby reducing computational complexity and memory usage.

Taken together, these findings highlight the practicality of ATSV. While HOSVD is computationally faster, its significantly lower estimation accuracy limits its utility. On the other hand, both HOOI and Tucker-L2E are sensitive to rank settings and may produce unstable results when the true rank is unknown or misestimated. ATSV overcomes these limitations by eliminating the need for rank specification altogether, reducing the burden on users and simplifying implementation. ATSV can be easily incorporated into real-world processing pipelines, where tensor decomposition serves as an intermediate step within ongoing data workflows, does not rely on manual intervention or extensive parameter tuning.

Nonetheless, the current form of ATSV does not guarantee exact recovery of the true low-rank tensor, and theoretical consistency in the asymptotic sense remains to be formally established. Future work should focus on clarifying whether the method achieves asymptotic convergence as sample size increases or noise diminishes. Furthermore, the noise model

used in this study assumes zero-mean i.i.d. Gaussian noise, which may not reflect the complexity of real-world data that could include non-Gaussian noise, outliers, or structured temporal or spatial correlations. Assessing the method’s reliability under such realistic conditions is an essential step toward enhancing its practicality and generalizability.

Although ATSV draws upon statistically grounded principles established in matrix-based singular value thresholding, its theoretical guarantees for tensor data remain to be established. In particular, the consistency and optimality of the method under high-dimensional and finite-sample tensor settings are still open questions. Verifying and strengthening the algorithm’s performance in these contexts will be a crucial direction for future work. Furthermore, as this study focused exclusively on synthetic simulations, further validation on real-world datasets—where challenges such as missing values, heteroscedasticity, and distributional shifts are common—will be important for confirming the method’s practical reliability and usability.

The academic significance of this work lies in the introduction of a novel framework that addresses the long-standing trade-off between estimation accuracy and computational burden in tensor decomposition. By leveraging singular value thresholding across tensor modes without iterative refinement, ATSV enables efficient and accurate low-rank approximation while preserving the structure of the original data. Compared to conventional iterative approaches, this framework offers a transparent and lightweight alternative, which avoids heuristic rank selection and convergence tuning. This contribution represents a step forward in tensor analysis methodology, offering both theoretical clarity and practical applicability.

From a practical standpoint, ATSV’s simplicity and parameter-free design confer substantial advantages for deployment in real-world scenarios. In contrast to traditional methods that require expert tuning and complex parameter configuration, ATSV allows non-specialists to conduct reliable analysis without sacrificing performance. Its lightweight algorithmic form also facilitates integration into existing systems and pipelines, supporting fast and reproducible data processing even in time-critical applications. From a user-centric perspective, ATSV eliminates the trial-and-error process often required for selecting appropriate ranks and tuning iterative solvers, thereby significantly reducing the barrier to entry for non-experts in tensor analysis. Moreover, the transparent and modular structure of the algorithm makes it well-suited for incorporation into large-scale monitoring systems or automated workflows. In this way, ATSV not only improves analytical outcomes but also provides a sustainable and scalable solution for real-world data processing challenges.

6 Conclusion

This study addressed the question of whether it is possible to efficiently and stably extract meaningful information from high-dimensional noisy data using a non-iterative, rank-free tensor decomposition method. To this end, we proposed Auto Tensor Singular Value Thresholding (ATSV), and quantitatively validated its effectiveness through simulation experiments. ATSV applies singular value thresholding to each mode unfolding of an observed tensor, automatically extracting statistically significant components while preserving the multi-dimensional structure of the data. Comparative evaluations under three different SNR conditions revealed that ATSV offers a superior balance among estimation accuracy, computational efficiency, and stability, with particularly notable advantages under low-SNR scenarios.

From an academic perspective, ATSV overcomes the classical trade-off between precision and computational cost that has long challenged conventional tensor decomposition techniques. By integrating non-iterative processing, parameter-free design, and automatic rank estimation into a unified framework, ATSV demonstrates that reliable and scalable low-rank approximation can be achieved without manual tuning. This framework holds promise as a bridge between mathematical theory and real-world implementation, with potential applications spanning large-scale data analysis, combinatorial optimization, and decision-support systems.

Practically, ATSV exhibits broad applicability in domains requiring the direct analysis of multi-dimensional data in tensor form. This includes sensor fusion in smart cities, anomaly detection in biomedical signals, and compression of high-frequency trading data in financial markets. Particularly in data environments involving spatial, temporal, and contextual dimensions—such as sensor networks and EEG recordings—ATSV enables stable inference without relying on iterative procedures or manual parameter adjustment. These characteristics substantially lower the barriers to practical deployment, positioning ATSV as a foundational technology for accelerating the practical use of tensor-based analytics.

Future research should address several open directions. Theoretical investigations are needed to establish the consistency and convergence properties of ATSV under asymptotic conditions. Furthermore, systematic evaluation is necessary to assess its performance under non-Gaussian noise or structurally dependent distortions—conditions frequently observed in real-world datasets. Beyond theory, expanding the number of real-world application cases is an urgent priority, as empirical evidence from practical deployments will further enhance the credibility and generalizability of the method. Given its modular nature, ATSV can potentially be extended to handle sparse tensors, missing entries, or online

processing scenarios. Integrating ATSV with temporal or graph-structured regularizations also opens up opportunities for enhancing contextual awareness in complex datasets. Through such advancements, ATSV is expected to evolve into a standard tool for tensor decomposition, contributing to both theoretical development and practical adoption. Ultimately, this study advances the frontier of tensor-based information extraction, and ATSV is anticipated to serve as a transformative core technology at the intersection of data science and real-world applications.

7 Acknowledgments

This work was supported by JSPS KAKENHI Grant Number 23K22166. During the preparation of this work, the authors used ChatGPT-4o to improve the quality of translation. After using this tool, the authors carefully reviewed and edited the content as needed and take full responsibility for the content of the publication.

8 Appendix

8.1 Lemmas

Lemma 1.

Let $\mathbf{Z}_n \in \mathbb{R}^{m \times n}$ be a matrix whose entries are i.i.d. standard Gaussian variables. The singular values of \mathbf{Z}_n follow the Marcenko–Pastur distribution, and the largest singular value converges almost surely to the so-called bulk edge:

$$\sigma_{\max}(\mathbf{Z}_n) \stackrel{\text{a.s.}}{=} 1 + \sqrt{\beta}, \quad \text{where } \beta = \frac{m}{n}.$$

This bulk edge represents the theoretical upper limit of singular values originating from noise and functions as a decision boundary in thresholding. If an observed singular value exceeds this limit, it is likely to correspond to a signal component rather than noise. According to Gavish and Donoho (2014), the optimal threshold τ^* should be set higher than this bulk edge to achieve effective denoising. The theoretical justification of Eq. (3) relies on the following two lemmas.

Lemma 2.

The asymptotic behavior of the observed singular value $y_{n,i}$ corresponding to the true singular value x_i is given by:

$$\lim_{n \rightarrow \infty} y_{n,i} = \begin{cases} \sqrt{\left(x_i + \frac{1}{x_i}\right) \left(x_i + \frac{\beta}{x_i}\right)}, & \text{if } x_i > \beta^{1/4}, \\ 1 + \sqrt{\beta}, & \text{if } x_i \leq \beta^{1/4}. \end{cases}$$

This result implies that when $x_i \leq \beta^{1/4}$, the corresponding observed singular value cannot be distinguished from noise. On the other hand, for $x_i > \beta^{1/4}$, the observed singular value emerges clearly from the noise bulk, indicating a recoverable signal.

Lemma 3.

The asymptotic alignment between the true left singular vector \mathbf{a}_i and the observed singular vector $\mathbf{u}_{n,j}$ satisfies:

$$d \cdot \lim_{n \rightarrow \infty} |\langle \mathbf{a}_i, \mathbf{u}_{n,j} \rangle|^2 = \frac{x_i^4 - \beta}{x_i^4 + \beta x_i^2}, \quad \text{for } x_i > \beta^{1/4},$$

and similarly for the right singular vectors:

$$d \cdot \lim_{n \rightarrow \infty} |\langle \mathbf{b}_i, \mathbf{v}_{n,j} \rangle|^2 = \frac{x_i^4 - \beta}{x_i^4 + x_i^2}, \quad \text{for } x_i > \beta^{1/4}.$$

In contrast, for $x_i \leq \beta^{1/4}$, the following holds:

$$\lim_{n \rightarrow \infty} |\langle \mathbf{a}_i, \mathbf{u}_{n,j} \rangle| = 0, \quad \lim_{n \rightarrow \infty} |\langle \mathbf{b}_i, \mathbf{v}_{n,j} \rangle| = 0, \quad \text{for all } j.$$

These results indicate that the recoverability of singular vectors is critically dependent on whether x_i exceeds the threshold $\beta^{1/4}$. This plays a significant role in determining the estimation accuracy of the low-rank components.

8.2 Asymptotic Mean Squared Error (AMSE)

The Asymptotic Mean Squared Error (AMSE) evaluates the limiting estimation error as the sample size tends to infinity. It is defined as:

$$\text{AMSE}(\hat{\mathbf{X}}_n) = \lim_{n \rightarrow \infty} \left\| \hat{\mathbf{X}}_n - \mathbf{X}_n \right\|_F^2. \quad (9)$$

Using inner product expansions:

$$\left\| \hat{\mathbf{X}} - \mathbf{X} \right\|_F^2 = \langle \hat{\mathbf{X}}, \hat{\mathbf{X}} \rangle + \langle \mathbf{X}, \mathbf{X} \rangle - 2\langle \hat{\mathbf{X}}, \mathbf{X} \rangle, \quad (10)$$

Each term is computed as:

$$\left\| \hat{\mathbf{X}} \right\|_F^2 = \sum_{i=1}^m \eta_H^2(y_i; \tau), \quad (11)$$

$$\left\| \mathbf{X} \right\|_F^2 = \sum_{i=1}^{r_{\max}} x_i^2, \quad (12)$$

$$\langle \hat{\mathbf{X}}, \mathbf{X} \rangle = \sum_{i=1}^m \sum_{j=1}^{r_{\max}} \eta_H(y_i; \tau) x_j \cdot \langle \mathbf{u}_i, \mathbf{a}_j \rangle \cdot \langle \mathbf{v}_i, \mathbf{b}_j \rangle. \quad (13)$$

Combining the above, we express the AMSE as:

$$\lim_{n \rightarrow \infty} \left\| \hat{\mathbf{X}} - \mathbf{X} \right\|_F^2 = \sum_{i=1}^m \eta_H^2(y_i; \tau) + \sum_{i=1}^{r_{\max}} x_i^2 - 2 \sum_{i=1}^m \sum_{j=1}^{r_{\max}} \eta_H(y_i; \tau) x_j \cdot \langle \mathbf{u}_i, \mathbf{a}_j \rangle \cdot \langle \mathbf{v}_i, \mathbf{b}_j \rangle.$$

Following Gavish and Donoho (2014), this can be rewritten as:

$$\lim_{n \rightarrow \infty} \left\| \hat{\mathbf{X}}_n - \mathbf{X}_n \right\|_F^2 = \sum_{i=1}^{r_{\max}} M(\hat{\mathbf{X}}_n, x_i), \quad (14)$$

where $M(\hat{\mathbf{X}}_n, x)$ denotes the AMSE contribution of the i -th singular value:

$$M(\hat{\mathbf{X}}_n, x) = \begin{cases} \left(x + \frac{1}{x}\right) \left(x + \frac{\beta}{x}\right) - \left(x^2 - \frac{2\beta}{x^2}\right), & x \geq x^*(\lambda), \\ x^2, & x < x^*(\lambda), \end{cases}$$

and the critical point $x^*(\lambda)$ is defined by:

$$x^*(\lambda) = \frac{\sqrt{\lambda^2 - \beta - 1} + \sqrt{(\lambda^2 - \beta - 1)^2 - 4\beta}}{2}.$$

8.3 About pseudo code

8.3.1 Optimal Singular Value Hard Thresholding Coefficient

Algorithm 2 Optimal Singular Value Hard Thresholding Coefficient

Input: Aspect ratio β , noise flag `sigma_known`

Output: Threshold coefficient τ

- 1: **if** `sigma_known` is True **then**
 - 2: $w \leftarrow \frac{8\beta}{\beta+1+\sqrt{\beta^2+14\beta+1}}$
 - 3: $\tau \leftarrow \sqrt{2(\beta+1)} + w$
 - 4: **else**
 - 5: $\tau_{\text{known}} \leftarrow \text{OptimalSVHTCoef}(\beta, \text{True})$
 - 6: $\mu \leftarrow \text{MedianMarcenkoPastur}(\beta)$
 - 7: $\tau \leftarrow \tau_{\text{known}} / \sqrt{\mu}$
 - 8: **end if**
 - 9: **return** τ
-

8.3.2 Median of the Marčenko–Pastur Distribution

Algorithm 3 Median of the Marčenko–Pastur Distribution

Input: Aspect ratio β

Output: Median value μ

```

1:  $a \leftarrow (1 - \sqrt{\beta})^2, b \leftarrow (1 + \sqrt{\beta})^2$ 
2: while  $b - a > \varepsilon$  (e.g.,  $\varepsilon = 0.001$ ) do
3:   Partition  $[a, b]$  into 5 points  $x$ 
4:    $y \leftarrow 1 - \text{incMarPas}(x, \beta)$ 
5:   Update  $a, b$  based on  $y$ 
6: end while
7: return  $(a + b)/2$ 

```

8.3.3 Incomplete Integral of the Marčenko–Pastur Distribution

Algorithm 4 Incomplete Integral of the Marčenko–Pastur Distribution

Input: Evaluation point x_0 , aspect ratio β , exponent parameter γ (default 0)

Output: Incomplete integral value I

```

1: if  $\beta > 1$  then
2:   Raise error:  $\beta$  must be in  $(0, 1]$ 
3: end if
4:  $a \leftarrow (1 - \sqrt{\beta})^2, b \leftarrow (1 + \sqrt{\beta})^2$ 
5: Define  $\rho(x) \leftarrow \frac{1}{2\pi\beta x} \sqrt{(b-x)(x-a)}$ 
6: Define integrand  $f(x) \leftarrow x^\gamma \cdot \rho(x)$ 
7: Compute  $I \leftarrow \int_{x_0}^b f(x) dx$  (e.g., Simpson's rule)
8: return  $I$ 

```

References

- [1] Haven, Emmanuel and Liu, Xiaoquan and Shen, Liya. De-noising option prices with the wavelet method. *European Journal of Operational Research*, 222(1):104–112, 2012.
- [2] Piramuthu, Selwyn. Evaluating feature selection methods for learning in data mining applications. *European journal of operational research*, 156(2):483–494, 2004.
- [3] Syberfeldt, Anna and Ng, Amos and John, Robert I and Moore, Philip. Evolutionary optimisation of noisy multi-objective problems using confidence-based dynamic resampling. *European Journal of Operational Research*, 204(3):533–544, 2010.
- [4] Badunenko, Oleg and Kumbhakar, Subal C. When, where and how to estimate persistent and transient efficiency in stochastic frontier panel data models. *European Journal of Operational Research*, 255(1):272–287, 2016.
- [5] Kilmer, Misha and Horesh, Lior and Avron, Haim and Newman, Elizabeth. Tensor-tensor products for optimal representation and compression. *arXiv preprint arXiv:2001.00046*, 2019.
- [6] Auddy, Arnab and Xia, Dong and Yuan, Ming. Tensor methods in high dimensional data analysis: Opportunities and challenges. *arXiv preprint arXiv:2405.18412*, 2024.
- [7] Kolda, Tamara G and Bader, Brett W. Tensor decompositions and applications. *SIAM review*, 51(3):455–500, 2009.
- [8] Fanaee-T, Hadi and Gama, João. Tensor-based anomaly detection: An interdisciplinary survey. *Knowledge-based systems*, 98:130–147, 2016.
- [9] Acar, Evrim and Dunlavy, Daniel M and Kolda, Tamara G and Mørup, Morten. Scalable tensor factorizations for incomplete data. *Chemometrics and Intelligent Laboratory Systems*, 106(1):41–56, 2011.
- [10] Zhang, Zemin and Aeron, Shuchin. Exact tensor completion using t-SVD. *IEEE Transactions on Signal Processing*, 65(6):1511–1526, 2016.

- [11] Carroll, J Douglas and Chang, Jih-Jie. Analysis of individual differences in multidimensional scaling via an N-way generalization of “Eckart-Young” decomposition. *Psychometrika*, 35(3):283–319, 1970.
- [12] Harshman, Richard A and others. Foundations of the PARAFAC procedure: Models and conditions for an “explanatory” multi-modal factor analysis. *UCLA working papers in phonetics*, 16(1):84, 1970.
- [13] Tucker, Ledyard R. Some mathematical notes on three-mode factor analysis. *Psychometrika*, 31(3):279–311, 1966.
- [14] Oseledets, Ivan V. Tensor-train decomposition. *SIAM Journal on Scientific Computing*, 33(5):2295–2317, 2011.
- [15] Zhao, Qibin and Zhou, Guoxu and Zhang, Liqing and Cichocki, Andrzej and Amari, Shun-Ichi. Bayesian robust tensor factorization for incomplete multiway data. *IEEE transactions on neural networks and learning systems*, 27(4):736–748, 2015.
- [16] Vervliet, Nico and De Lathauwer, Lieven. A randomized block sampling approach to canonical polyadic decomposition of large-scale tensors. *IEEE Journal of Selected Topics in Signal Processing*, 10(2):284–295, 2015.
- [17] Xue, Niannan and Papamakarios, George and Bahri, Mehdi and Panagakakis, Yannis and Zafeiriou, Stefanos. Robust low-rank tensor modelling using Tucker and CP decomposition. *2017 25th European Signal Processing Conference (EUSIPCO)*, 1185–1189, 2017.
- [18] Erichson, N Benjamin and Manohar, Krithika and Brunton, Steven L and Kutz, J Nathan. Randomized CP tensor decomposition. *Machine Learning: Science and Technology*, 1(2):025012, 2020.
- [19] De Lathauwer, Lieven and De Moor, Bart and Vandewalle, Joos. A multilinear singular value decomposition. *SIAM journal on Matrix Analysis and Applications*, 21(4):1253–1278, 2000.
- [20] De Lathauwer, Lieven and De Moor, Bart and Vandewalle, Joos. On the best rank-1 and rank-(r_1, r_2, \dots, r_n) approximation of higher-order tensors. *SIAM journal on Matrix Analysis and Applications*, 21(4):1324–1342, 2000.
- [21] Tomioka, Ryota and Suzuki, Taiji and Hayashi, Kohei and Kashima, Hisashi. Statistical performance of convex tensor decomposition. *Advances in neural information processing systems*, 24, 2011.
- [22] Goldfarb, Donald and Qin, Zhiwei. Robust low-rank tensor recovery: Models and algorithms. *SIAM Journal on Matrix Analysis and Applications*, 35(1):225–253, 2014.
- [23] Jang, Jun-Gi and Kang, U. Fast and memory-efficient tucker decomposition for answering diverse time range queries. *Proceedings of the 27th ACM SIGKDD Conference on Knowledge Discovery & Data Mining*, 725–735, 2021.
- [24] Heng, Qiang and Chi, Eric C and Liu, Yufeng. Robust low-rank tensor decomposition with the L2 criterion. *Technometrics*, 65(4):537–552, 2023.
- [25] Bai, Mingyuan and Choy, ST Boris and Song, Xin and Gao, Junbin. Tensor-Train Parameterization for Ultra Dimensionality Reduction. *2019 IEEE International Conference on Big Knowledge (ICBK)*, 17–24, 2019.
- [26] Sofuoğlu, Seyyid Emre and Aviyente, Selin. Graph regularized tensor train decomposition. *ICASSP 2020-2020 IEEE International Conference on Acoustics, Speech and Signal Processing (ICASSP)*, 3912–3916, 2020.
- [27] Li, Lingjie and Yu, Wenjian and Batselier, Kim. Faster tensor train decomposition for sparse data. *Journal of Computational and Applied Mathematics*, 405:113972, 2022.
- [28] Zhou, Yuchen and Zhang, Anru R and Zheng, Lili and Wang, Yazhen. Optimal high-order tensor svd via tensor-train orthogonal iteration. *IEEE transactions on information theory*, 68(6):3991–4019, 2022.
- [29] Aksoy, Doruk and Gorsich, David J and Veerapaneni, Shravan and Gorodetsky, Alex A. An incremental tensor train decomposition algorithm. *SIAM Journal on Scientific Computing*, 46(2):A1047–A1075, 2024.
- [30] Hillar, Christopher J and Lim, Lek-Heng. Most tensor problems are NP-hard. *Journal of the ACM (JACM)*, 60(6):1–39, 2013.
- [31] Gavish, Matan and Donoho, David L. The optimal hard threshold for singular values is $4/\sqrt{3}$. *IEEE Transactions on Information Theory*, 60(8):5040–5053, 2014.
- [32] Vannieuwenhoven, Nick and Vandebril, Raf and Meerbergen, Karl. A new truncation strategy for the higher-order singular value decomposition. *SIAM Journal on Scientific Computing*, 34(2):A1027–A1052, 2012.
- [33] Zhang, Anru and Xia, Dong. Tensor SVD: Statistical and computational limits. *IEEE Transactions on Information Theory*, 64(11):7311–7338, 2018.